Diversity of Hydrogen Bond Network and Its Impact on NMR Parameters of Amylose B Polymorph. A Study Using Molecular Dynamics and DFT Calculations Within Periodic Boundary Conditions

Adrien Schahl, I.C. Gerber, Réat Valérie, Franck Jolibois

Diversity of Hydrogen Bond Network and Its Impact on NMR Parameters of Amylose B Polymorph. A Study Using Molecular Dynamics and DFT Calculations Within Periodic Boundary Conditions.

Adrien Schahl[a,b], Iann C. Gerber[a], Valérie Réat[b] and Franck Jolibois[a]*

(a) A.Schahl, I.C.Gerber and F.Jolibois, LPCNO, CNRS UMR 5215, Université de Toulouse-INSA-UPS, 135 av. Rangueil, F-31077, Toulouse, France, franck.jolibois@univ-tlse3.fr

(b) A.Schahl and V.Réat Institut de Pharmacologie et Biologie Structurale, UMR 5089, CNRS–Université de Toulouse-UPS BP 64182, 205 route de Narbonne, 31077 Toulouse, Cedex 04, France

KEYWORDS Starch • Amylose • DFT • Molecular dynamics • Periodic Boundary Conditions

Abstract.

Classical molecular dynamics simulations have been combined to quantum (DFT) calculations of ^{13}C NMR parameters in order to relate the experimental spectrum of the double–helix form of the amylose B-polymorph in highly crystalline conditions not only to its 3D structure but also to the arrangement of atoms in the crystal lattice. Structures obtained from these simulations or from geometry optimizations procedure at the DFT level have shown the presence of hydrogen bond networks between sugars of the same helix or between residues of the two chains of the double helix. ^{13}C NMR parameter calculations have revealed the impact of such network on the chemical shifts of carbon atoms. In addition, DFT calculations using periodic boundary conditions were compulsory to highlight the presence of two types of sugar within the crystal sample. It allows us to confirm theoretically, the experimental hypothesis that the existence of two distinct sugar types in the NMR spectrum is a consequence of crystal packing.

Introduction.

Amylose, one of the major constituents of starch with amylopectin, is an essentially linear polymer composed of glucose residues linked in [α-1→4] and is often used to model the crystalline parts of starch. Most of the experimental structures are originated from X-ray diffraction studies[1–4] and it is well known that it can adopt different helical conformations, depending on its environment. The single helical structure called the V-polymorph, has been proven to encapsulate guest molecules of various sizes, such as Iodine[5], flavor molecules[6,7] or even fatty acids[8–11]. The double helical structures are called A or B-polymorphs (Figure 1) depending on the crystal packing conditions and are known to be present in highly crystalline material amongst starch. The method of choice used for the study of amylose structure is ^{13}C solid-state NMR spectroscopy[9,10,12–14],

allowing to differentiate between these polymorphs. It is especially known that chemical shifts of the C_1 and C_4 carbon atoms are the most affected by the dihedral angles of the glycosidic linkage (see Figure 1 for atom numbering and definition of angles). At the same time, chemical shift of the other carbon atoms (C_2, C_3, C_5 and C_6) are mainly affected by the presence and the nature of hydrogen bonds involving the hydroxyl groups and by the associated dihedral angles[15,16].

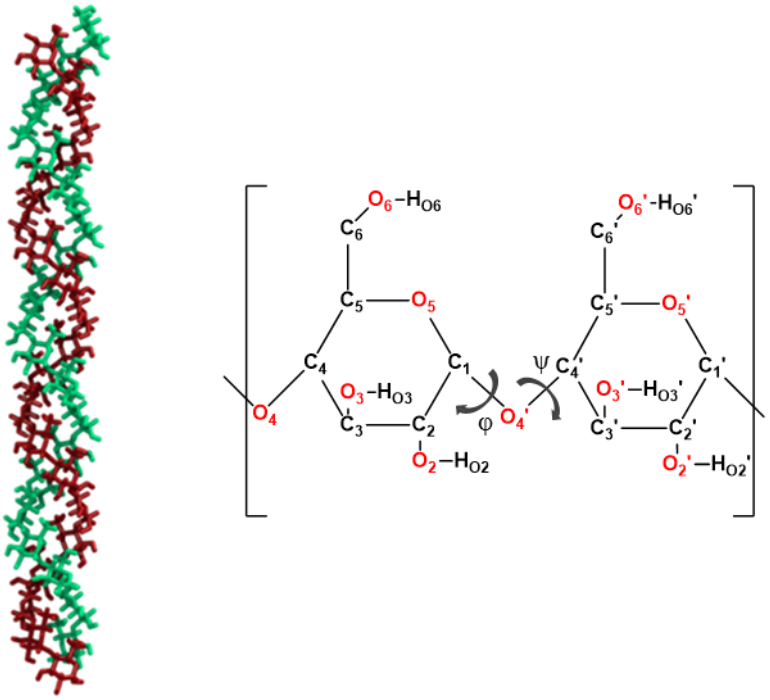

Figure 1. (Left) 3D Structure of the B-type Amylose. (Right) Atom numbering and definition of glycosidic dihedral angles φ = O_5-C_1-O_4'-C_4' and ψ = C_1-O_4'-C_4'-C_3'.

If the general spectrum of the B-polymorph has been known for a long time, it is only since 2006 that the precise NMR spectrum assignment has been performed on a sample uniformly ^{13}C labelled and presenting a high crystallinity[17]. Particularly, it reveals the presence of two different signals for the C_1, C_2, C_4 and C_5 carbons that witness the presence of two different glucose residues. This observation of two different monomers characteristic of this amylose polymorph was related to the

crystal packing conditions. However, the link between the molecular structure and the environment leading to two different NMR signatures remains unknown.

Theoretical studies of the structures of amylose have been undertaken but they are mainly based on the use of classical molecular dynamics (MD). The development of force fields[18–20] dedicated to carbohydrates has greatly facilitated such studies. They have helped to study changes in the conformation of amylose in different environments[21,22], as well as the complexation process occurring between fatty acids and amylose polymers of different degree of polymerization (DP)[23–26]. Computational studies using quantum chemical methods for the calculations of NMR parameters have mainly been focused on relatively small systems[27]. It is only recently that larger systems have been studied, such as cellulose clusters[28–30] or medium size amylose-lipids complexes[31]. In the past decades, *ab initio* or DFT-based quantum chemical approaches using the Gauge Including Atomic Orbital (GIAO)[32] method have been widely used for the calculations of ^{13}C chemical shielding tensors. In the context of polysaccharides, these methods are especially useful as they allow precise reproduction of experimental ^{13}C chemical shifts and correlation between 3D structural changes and evolution of chemical shielding tensors[27,31]. However, if this method behaves successfully in reproducing NMR parameters of molecular systems, important effects due to packing conditions are missing if crystalline systems are considered. A common way to circumvent this problem is to take into account long-range order effects using DFT calculations within periodic boundary conditions (PBC). For the special case of carbon chemical shielding tensor calculations, the Gauge Including Projected Augmented Wave (GIPAW)[33,34] is the method of choice that has already proved its robustness either for small molecules[35,36], or for bulk calculations[37–39]. To the best of our knowledge, this method has never been used for the calculation of NMR parameters of polysaccharides.

Here we present a study that relates ^{13}C chemical shifts of the B-polymorph of amylose to its 3D structure and its major interactions. We used a combination of DFT and classical molecular dynamics calculations to generate structures for the theoretical computation of NMR parameters. We show that the use of molecular methods is not sufficient to capture the main features of the experimental ^{13}C chemical shifts, thus confirming that this effect is not due to structural differences inside the complex. However, this computational study highlights the impact of the hydrogen bond network (HBN) on the calculations of NMR parameters of such systems. As we refer to experimental data obtained on a crystalline material, we have intensively used the GIPAW methodology. It allowed us to differentiate between two different types of residue placed alternately along each amylose chain and to link their position in the crystal to the two distinct glucose NMR signals experimentally identified.

Methods.

Classical molecular dynamics. Molecular dynamics simulations were performed using the NAMD software[40]. The initial structure of the double chain of amylose has been constructed with the leap program of the AMBER suite[41] using geometrical input parameters corresponding to X-ray crystallographic double helical structure of B-Amylose[42]. Two independent chains of 20 residues were first generated resulting in helices with a distribution of dihedral angles phi ($\varphi = O_5$-C_1-O_4'-C_4') and psi ($\psi = C_1$-O_4'-C_4'-C_3') around 91.2° ± 3.5° and 91.8° ± 3.2°, respectively. One of these chains was then rotated by 180° around its principal axis of inertia using the Avogadro software[43] in order to obtain a double helix close to the B-polymorph X-ray crystallographic structure. The procedure for solvation and molecular dynamics was the same as recently described[31]. Amylose was solvated in a box of water such that it was placed at 20 Å from the box boundaries. A modified version of GLYCAM06 force field[31] and the TIP3P model were used for

the description of the amylose and the water molecules respectively. The production run was carried out during 55 ns in the canonical ensemble (NVT) with atomic coordinates frame saved every picosecond.

In order to analyze the dynamic of specific chemical groups, density maps have been calculated regarding some specific dihedral angles (see Results and discussion section for details). These plots were realized as follow: dihedral angles of interest were sampled each 10 ps. Then the population of each couple of angles were classified in two-dimensional arrays with angles going from 0° to 360° with a step of 0.6°. A probability density function was then calculated through the use of the gaussian_kde module of the scipy python library[44]. The value of this function is depicted through the color scale situated next to density maps.

Quantum chemical calculations – Molecular approach. All calculations were performed using Gaussian09 suite of programs[45]. Geometry optimisations and spectroscopic properties calculation have been performed at the DFT level using B3LYP[46,47] hybrid functional associated to the 6-31G(d,p) basis set[48,49]. For the computation of isotropic chemical shielding, the GIAO method[50] has been employed for the numerous advantages it offers. Calculations of NMR parameters were carried out considering a molecular approach. In a first case, ^{13}C chemical shielding calculations were performed using a full quantum chemical computational strategy, i.e., NMR calculations on structures obtained by geometry optimisations. First, full geometry optimisation (optimisation of all atomic positions) has been performed. In this special case, implicit solvent effects (water solvent) were taken into account using the Integral Equation Formalism variant of the Polarizable Continuum Model (IEFPCM[51]). This was compulsory to maintain the 4 terminal residues in a conformation close to the B-polymorph. The starting geometry was obtained from the "Centre de Recherche sur les Macromolecules Végétales (CERMAV)" website[52,42]. One double helix was

extracted from the crystallographic data set. It is made of two chains of six glucose residues. Hydrogens of hydroxyl groups have been added with the automatic tool of the Avogadro software[43]. It is well known that the nature and orientation of hydrogen bonds have an impact over calculations of NMR parameters in the case of carbohydrate systems[15]. If two consecutive glucose residues are considered, two types of hydrogen bonds can be envisaged: On one hand the hydrogen of the O_3H hydroxyl group can interact with the oxygen of the O_2H hydroxyl group of the following glucose. On the other, the hydrogen of the O_2H hydroxyl group can interact with the oxygen of the O_3H hydroxyl group of the previous glucose. Consequently, two starting structures with different hydrogen bond network were considered for geometry optimisations. One (noted HBN_1) is formed by hydrogen bonds between $H_{O3}{}^{(n)}$ and $O_2{}^{(n+1)}$, $H_{O2}{}^{(n+1)}$ and $O_6{}^{(m)}$, $H_{O6}{}^{(m)}$ and $O_5{}^{(m+1)}$, with n being the numbering of considered residues of one chain and m being the numbering of residues composing the other chain (Figure 2A). The other (noted HBN_2) is formed by hydrogen bonds between $H_{O6}{}^{(m)}$ and $O_2{}^{(n+1)}$ and $H_{O2}{}^{(n+1)}$ and $O_3{}^{(n)}$ (Figure 2B). In addition to full geometry optimisation procedure, constrained geometry optimisations have also been undertaken to keep the crystallographic position of heavy atoms, as the NMR experimental data refer to a crystalline material. Under these conditions, only the positions of the hydrogen atoms have been optimized for the two different hydrogen bond networks.

In a second stage, because it is known that molecular dynamics have an impact on structures and spectroscopic parameters[31], calculations of NMR parameters have been performed on 100 structures extracted from the molecular dynamics trajectory. To avoid border effects, 24 residues over 40 have been selected in the middle part of B-amylose in order to obtain two chains of 12 residues folded in a double helix fashion. The 4 terminal residues have been completed with hydrogen atoms linked either to the O_4 or the O_1 oxygen atoms.

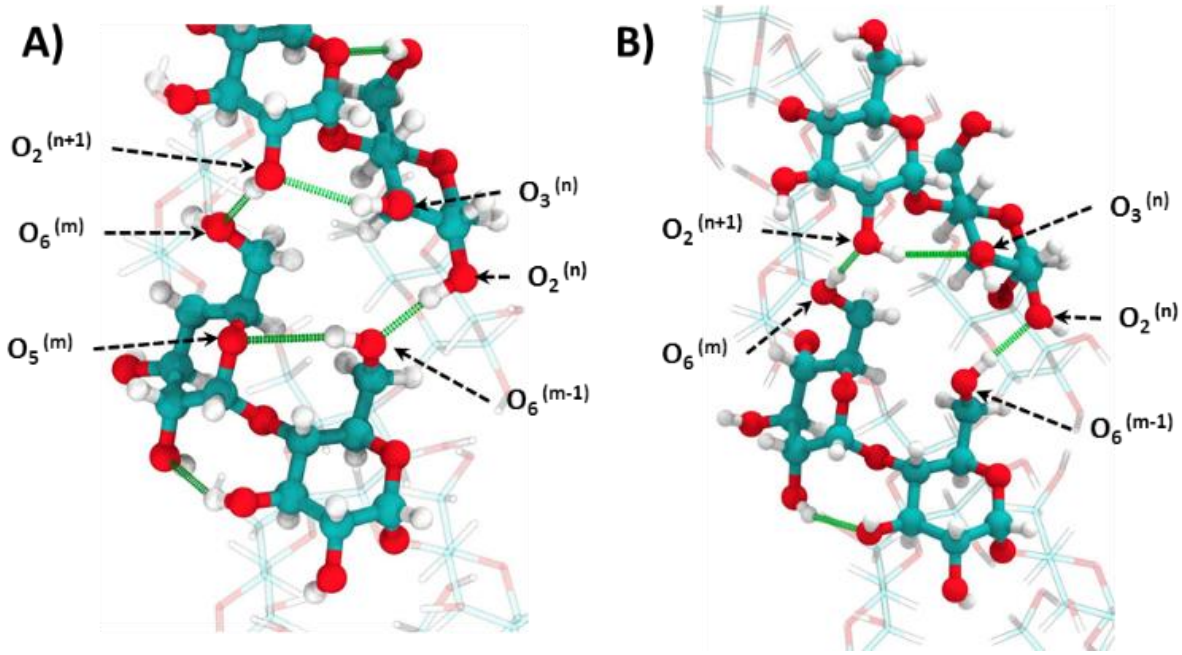

Figure 2. A) Hydrogen bond network 1 (HBN_1) B) Hydrogen bond network 2 (HBN_2). The two structures presented are resulting from geometry optimizations of all the atoms positions.

In order to determine theoretical chemical shifts, it is necessary to calculate the difference between nuclear shielding of a probed nucleus and the one of the same nucleus in a reference compound (TMS for ^{13}C NMR spectroscopy). To achieve this, it is necessary to calculate the chemical shielding of the reference at the same theoretical level as that used to calculate the chemical shielding of the sample. In our case, because several theoretical levels have been used, this procedure is not the most relevant. Instead, we have plot experimental isotropic chemical shift as a function of calculated isotropic chemical shielding. Linear fitting of this plot allows us to extract the slope and the intercept which are used to calculate the theoretical chemical shifts. The slope of this linear correlation allows correcting our data from weakness of the theoretical model (mainly absence of environment effects) and the intercept corresponds to the reference shielding used to transform chemical shielding into chemical shift.

Quantum chemical calculations - periodic boundary conditions. Periodic DFT calculations were carried out using the Vienna ab initio simulation package VASP[53–56]. The code uses the full-potential projector augmented wave (PAW) framework[57,58]. Exchange-correlation effects have been approximated using the Perdew-Burke-Ernzerhof (PBE) functional[59] and completed by Grimme D3 scheme[60] to account for van der Waals forces. A kinetic-energy cut-off of 500 eV was found to be sufficient to achieve a total-energy convergence within several meV, considering a k-point sampling of (2x2x3) for the structure's optimization, in conjunction with a Gaussian smearing with a width of 0.05 eV (See Figure S1). Force convergence criteria have been set to 0.01 eV/Å on each relaxed atom. Periodic calculations of nuclear shielding have been performed within the GIPAW approach[33,34] as implemented in the VASP package[61], using a gamma only (1x1x1) k-point grid for the integration of the Brillouin zone, since the use of denser grids has a very limited impact on the result's accuracy. Indeed, as an example, a difference of less than 1 ppm is observed when a (2x2x3) k-point grid is used (data not shown). For these calculations, the molecular system consisted in a 3D cell constituted with two left-handed, parallel-stranded double helices. The cell parameters (hexagonal space group with a=b=18.5 Å and c=10.4 Å) and atomic coordinates (252 atoms) were obtained and generated according to the X-ray crystallographic structure[42]. As in the previous molecular case, theoretical shieldings were transposed into chemical shifts using the parameters of the linear correlation between theoretical and experimental data.

Results and Discussion.

Standard molecular approach. In a first attempt to reproduce carbon experimental chemical shifts of the B-type double helix structure of amylose, calculations have been performed using a standard approach, i.e., spectroscopic parameters calculated on optimized geometry of isolated molecular system (see computational details). To account for dynamical effects on spectroscopic

parameters, carbon chemical shielding averaged over a set of structures extracted from molecular dynamics have also been considered.

All values obtained for each selected dihedral angle are displayed in tables S1 - S3 for geometry optimisations and in table S4 and S5 for MD simulations. From a structural point of view, the average value of selected dihedral angles was calculated along the glucose chains and, when necessary, along the MD simulation. This was done to identify the hydrogen bond networks and the structural features of amylose chains in B-polymorph.

	Opt_{HBN_1}	Opt_{HBN_2}	$Opt_{HBN\_1}(H)$	$Opt_{HBN\_2}(H)$
O_5-C_1-O_4'-C_4'	94.7 ± 4.6	95.3 ± 6.1	84.0 ± 0.1	84.0 ± 0.1
C_1-O_4'-C_4'-C_3'	97.8 ± 6.1	94.7 ± 4.0	94.2 ± 0.1	94.2 ± 0.1
C_4-C_5-C_6-O_6	48.6 ± 8.7	57.7 ± 3.0	59.6 ± 8.2	59.6 ± 8.2
C_1-C_2-O_2-H_{O2}	227.9 ± 25.4	27.3 ± 3.8	278.8 ± 1.7	43.1 ± 5.2
C_2-C_3-O_3-H_{03}	188.7 ± 9.3	307.7 ± 3,6	202.3 ± 12.2	300.1 ± 7.7
C_5-C_6-O_6-H_{06}	284.9 ± 3.9	154.3 ± 8.7	284.3 ± 2.3	140.2 ± 4.8

Table 1. Selected averaged dihedral angles (degrees) of the full optimisations resulting in the HBN_1 (Opt_{H_BN1}) and in the HBN_2 (Opt_{H_BN2}) structures and of the optimisations restrained to hydrogens resulting in the $Opt_{H\_BN1}(H)$ and in the $Opt_{H\_BN2}(H)$) structures. O_5-C_1-O_4'-C_4' and C_1-O_4'-C_4'-C_3' are the φ and ψ angles (see Figure 1 for atom numbering), respectively. See Figure 1 for the definition of the hydrogen bond networks HBN_1 and 2.

Regarding the angles that characterise the anomeric bond (Tables 1 and S1), the optimised φ angles are on average 10° larger than in the crystallographic structure, while the corresponding angles ψ are almost not affected. In the case of MD simulation (Tables S4 and S5), even if these two angles are close to the crystallographic ones, the φ angles have a higher dynamic range with standard deviations that are systematically larger than the ψ angles. According to this, it appears

that the nature of the hydrogen bond network has little influence on the values of these glycosidic dihedral angles. The same conclusion can be reached for the dihedral angles around the C_5-C_6 bonds (Table 1), all glucose residues mainly adopting a *gg* conformation as already observed experimentally either on crystal structure[62] or by mean of ^{1}H NMR spectroscopy[63].

The dihedral angles associated to the hydrogen atoms of the three hydroxyl groups obviously correspond to structural features that can be used to differentiate the two hydrogen bond networks.

Geometry optimizations including all atoms or restrained to hydrogens do not have a drastic impact on the values of the characteristic dihedral angles for each hydrogen bonds network (Tables 1, S2 and S3). According to the description of each hydrogen bond network (Figure 2), regions of the configuration space can be highlighted. HBN_1 can be associated to the dihedral angles C_1-C_2-O_2-H_{O2}, C_2-C_3-O_3-H_{O3} and C_5-C_6-O_6-H_{O6} ranging from 200° to 280°, 180° to 215° and 280° to 290°, respectively. For HBN_2, another region of the configuration space is characterized with dihedral angles ranging from 25° to 50°, 290° to 310° and 135° to 165° for C_1-C_2-O_2-H_{O2}, C_2-C_3-O_3-H_{O3} and C_5-C_6-O_6-H_{O6}, respectively. The average values of the three dihedral angles were obtained while excluding the values of the residues 1, 2, 3 and 1' for the C_1-C_2-O_2-H_{O2} and C_2-C_3-O_3-H_{03} angles and 6, 4', 5' and 6' for the C_5-C_6-O_6-H_{06} (see details in Table S4). In our initial model, these particular hydroxyl groups have no residues facing them. Their conformations are therefore not representative of hydrogen bonding networks. For the MD simulations, the density maps between the dihedral angles C_1-C_2-O_2-$H_{O2}^{(n+1)}$ and C_2-C_3-O_3-$H_{O3}^{(n)}$ and the dihedral angles C_5-C_6-O_6-$H_{O6}^{(m)}$ and C_1-C_2-O_2-$H_{O2}^{(n)}$ (Figure 3) show maximum density values for C_1-C_2-O_2-$H_{O2}^{(n+1)}$, C_2-C_3-O_3-$H_{O3}^{(n)}$ and C_5-C_6-O_6-$H_{O6}^{(m)}$ around 80°, 275° and 145°, respectively. Despite substantial differences with the static quantum chemical structures (Table 1), these values are closer to the representative angles of the hydrogen bond network HBN_2. Furthermore, in the

density map, the C_5-C_6-O_6-H_{O6} dihedral angle values only are representative of the HBN_2 network (Table 1) attesting the formation of the $H_{O6}^{(m)} \cdots O_2^{(n+1)}$ hydrogen bond (Figure 2B, Figure 3A). This may indicate that this network is mainly present during the molecular dynamic simulation. The presence of a second maximum on the C_1-C_2-O_2-$H_{O2}^{(n+1)}$ and C_2-C_3-O_3-$H_{O3}^{(n)}$ density map at 170° and 190° may be an indicator, to a lesser extent, of the presence of the HBN_1 network. Yet, if it attests the formation of $H_{O3}^{(n)} \cdots O_2^{(n+1)}$ hydrogen bonds (Figure 2B), the location of the C_1-C_2-O_2-H_{O2} at 170° prevents the formation of $H_{O2}^{(n+1)} \cdots O_6^{(m)}$ hydrogen bond which is a characteristic of HBN_1. The presence of a non-negligible population of C_2-C_3-O_3-H_{O3} located around 190° (Figure 3B) associated to C_1-C_2-O_2-H_{O2} located around 170° proves, however, the ability of the system to start forming the HBN_1 network according to our simulation conditions (Table 1).

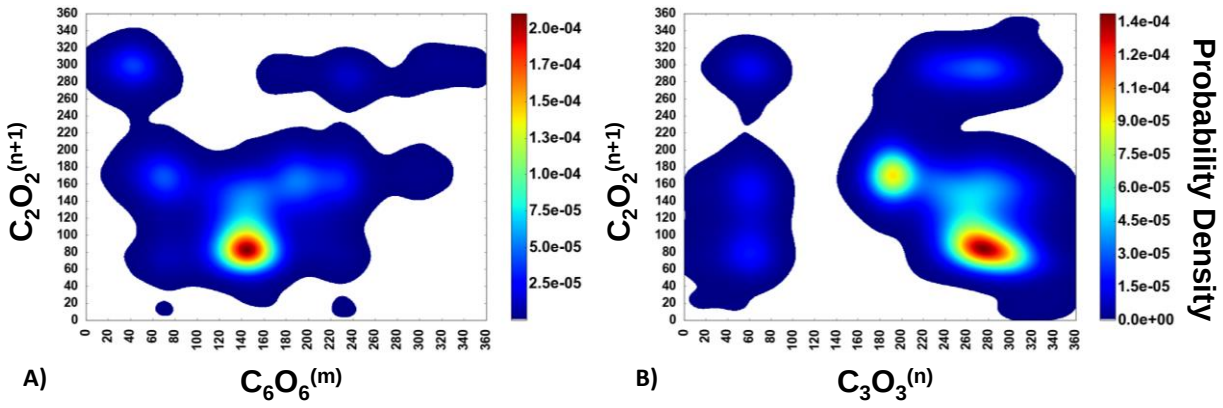

Figure 3. A) Density map for the couple of dihedral angles C_1-C_2-O_2-H_{O2} of residue n+1 (noted $C_2O_2^{(n+1)}$) and C_5-C_6-O_6-H_{O6} of residue m (noted $C_6O_6^{(m)}$). B) Density map for the couple of dihedral angles C_2-C_3-O_3-H_{O3} of residue n (noted $C_3O_3^{(n)}$) and C_1-C_2-O_2-H_{O2} of residue n+1 (noted $C_2O_2^{(n+1)}$). Angles are given in degrees.

Based on this analysis of conformational properties, molecular dynamics simulations of isolated B-type double helix of amylose indicate that even if one hydrogen bond network (HBN_2) is

mainly present, the second might also exist. The existence of these two hydrogen bond networks might be responsible for the two distinct sets of chemical shifts observed by NMR experiments[17] and that indicate the existence of two types of sugars within the polymer.

Using all the previously described molecular structures, ^{13}C chemical shift calculations were carried out (theoretical chemical shielding given in Tables S6 and S7 for optimised HBN_1 and 2 structures) and compared to experimental chemical shifts (Table S8). Correlation between theoretical and experimental data has failed to distinguish two sugars, as expected from experiment. Indeed, according to the distribution of the chemical shift values for each carbon (see Tables S6 and S7), no specific pattern has appeared that can allow to highlight two different sugars. As a consequence, the average chemical shieldings have been calculated for each carbon and compared to experiment. For C_2, C_3, C_5 and C_6, all residues have been considered for the average estimates while, in the case of C_1 and C_4, carbons attached to a hydroxyl group (sugars at the extremities of each chain) have not been taken into account. This set of 6 mean values of carbon chemical shielding was finally compared to the carbon chemical shifts characterizing one of the 2 types of glucose (noted Sugar 1 and 2) identified experimentally. Linear correlations between theoretical and experimental data have been performed and chemical shifts have been determined using the slope and the intercept of each linear fit (data reported in Tables 2 and S8). Finally, the root mean square differences (RMSD) have been calculated in order to give another criterion of computational accuracy. For each correlation, results (R^2 and RMSD) are given in Table 2. In addition, errors relative to experience are displayed in Figure 4.

	Sugar 1[17]	Opt_{HBN_1}	Opt_{HBN_2}	$Opt_{HBN\ 1}$ (H only)	$Opt_{HBN\ 2}$ (H only)	Mol. Dyn.
C1	**99.3**	98.9 (± 1.2)	98.4 (± 0.7)	98.5 (± 0.7)	98.9 (± 0.9)	98.3(±0.4)
C2	**71.3**	70.4 (± 0.6)	72.1 (± 0.6)	67.1 (± 0.3)	69.6 (± 0.3)	73.6(±0.5)
C3	**75.1**	71.3 (± 1.2)	73.9 (± 1.6)	77.6 (± 0.8)	76.6 (± 1.1)	72.3(±0.3)
C4	**72.6**	76.1 (± 1.8)	74.3 (± 1.1)	73.6 (± 0.3)	73.1 (± 0.6)	74.4(±0.7)
C5	**69.8**	70.9 (± 1.1)	71.3 (± 1.1)	69.4 (± 1.2)	69.8 (± 1.2)	71.0(±0.5)
C6	**61.3**	61.8 (±1.2)	59.5 (± 0.7)	63.1 (± 1.3)	61.4 (± 1.3)	59.7(±0.5)
R^2		0.965	0.987	0.965	0.994	0.974
RMSD		2.2	1.4	2.2	0.9	1.9
	Sugar 2[17]	Opt_{HBN_1}	Opt_{HBN_2}	$Opt_{HBN\ 1}$ (H only)	$Opt_{HBN\ 2}$ (H only)	Mol. Dyn.
C1	**100.2**	100.1 (± 1.2)	99.5 (± 0.7)	99.5 (± 0.7)	99.9 (± 0.9)	99.5 (± 0.4)
C2	**72.1**	70.9 (± 0.6)	72.7 (± 0.6)	67.6 (± 0.3)	70.2 (± 0.3)	74.2 (± 0.5)
C3	**75.1**	71.9 (± 1.2)	74.5 (± 1.6)	78.3 (± 0.8)	77.2 (± 1.1)	72.9 (± 0.3)
C4	**74.3**	76.7 (± 1.8)	74.9 (± 1.1)	74.2 (± 0.7)	73.7 (± 0.6)	75.1 (± 0.7)
C5	**70.2**	71.5 (± 1.1)	71.8 (± 1.1)	70.0 (± 1.2)	70.3 (± 1.2)	71.5 (± 0.5)
C6	**61.3**	62.2 (± 1.2)	59.8 (± 0.7)	63.6 (± 1.7)	61.8 (± 1.3)	60.0 (± 0.5)
R^2		0.976	0.993	0.958	0.990	0.984
RMSD		1.8	1.0	2.4	1.2	1.5

Table 2. Corrected values of averaged theoretical chemical shifts (ppm). Correlation coefficient and RMSD (ppm) between the corrected averaged theoretical chemical shifts and the experimental chemical shifts of Sugar 1 and Sugar 2. Opt_{HBN_1}, Opt_{HBN_2} or Opt_{HBN_1} (H only), Opt_{HBN_2} (H only) refer to geometry optimisations on all atoms or restrained to hydrogen atoms for the HBN_1 and HBN_2 structures, respectively. Mol. Dyn. refers to calculation performed on structures extracted from molecular dynamics simulations. Errors (standard deviations) are given in parenthesis.

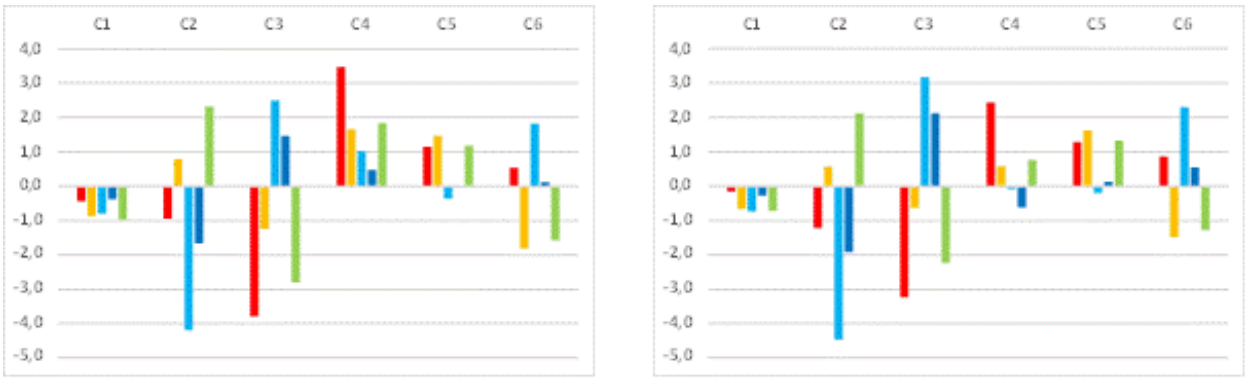

Figure 4. Relative errors (ppm) for each carbon atom of the glucose unit in comparison with Sugar 1 (left) and Sugar 2 (right). Red: Opt_{HBN_1}. Yellow: Opt_{HBN_2}. Light blue: Opt_{HBN_1}(H only). Dark blue: Opt_{HBN_2}(H only). Green: Mol. Dyn..Opt_{HBN_1}, Opt_{HBN_2} or Opt_{HBN_1} (H only), Opt_{HBN_2} (H only) refer to geometry optimisations on all atoms or restrained to hydrogen atoms for the HBN_1 and HBN_2 structures, respectively. Mol. Dyn. refers to calculation performed on structures extracted from molecular dynamics simulations.

Among all calculations, the HBN_2 structure appears to be the best if correlation coefficient and RMSD are considered (Figure 4 – yellow bars). It has been shown recently that the addition of dynamical effects by means of molecular dynamic simulations can improve the calculation of NMR spectra[31]. Therefore, this approach was applied to a B-polymorph model of 2 x 20 residues (see computational details). Adding dynamical effects was not sufficient to allow the differentiation of two specific sugars (Table S8). As previously done, linear fits of the average values were performed with either Sugar 1 or Sugar 2 experimental values (Table 2 – "Mol. Dyn." column and Figure 4 - Green bar). Despite a correct correlation with the Sugar 1 and Sugar 2 experimental values (R^2 = 0.974 and 0.984, RMSD= 1.9 and 1.5 ppm, respectively), introduction of dynamical effects did not allow to improve the previous NMR parameters calculated on optimized geometries. Because the relative atomic positions may have a significant impact on the

value of chemical shifts and may allow to discriminate two types of sugars within the B-type amylose, calculation of NMR parameters has been considered on the geometry obtained experimentally. In this case, solely the positions of hydrogen atoms have been optimised because their position is neither well defined experimentally nor defined at all in the case of hydroxyl groups. As previously observed, keeping the heavy atoms frozen to their crystallographic positions does not allow to differentiate two types of sugar regarding ^{13}C chemical shifts (Table S7). However, while the structure associated to the HBN_1 network presents a poor correlation with the experimental values (Table 2 "Opt_{HBN_1}(H)", R^2=0.965 and 0.958, RMSD=2.2 and 2.4 ppm for Sugar 1 and Sugar 2, respectively), the other one, associated to the HBN_2 network gives best results (Table 2 "Opt_{HBN_2}(H)", R^2=0.994 and 0.990, RMSD=0.9 and 1.2 ppm for Sugar 1 and Sugar 2, respectively). Even if this last structure seems to be in better agreement with experiment than the other one, it doesn't manage to reproduce correctly all individual carbon chemical shifts (in particular for C_2 and C_3 with relative errors between 1.5 and 2 ppm in absolute value). Furthermore, the fact that the correlation is good with the two types of sugar remains also questionable.

At this stage of our study, two conclusions can be underlined: 1) Despite a good overall correlation between calculated values and experimental ones, molecular methods are not sufficient to clearly discriminate two types of sugar in such systems. Thus, this difference may not be explained neither by a dynamical effect nor an intrinsic structural effect. 2) The hydrogen bond network inside one double helix has a non-negligible impact on the calculation of NMR parameters. Here, molecular methods suggest that the HBN_2 structure is responsible for the experimental chemical shift as far as there is no packing effect. Thus, the packing effect observed experimentally has to be somehow considered in the NMR calculation to allow this differentiation.

Periodic boundary conditions approach. Experimentally, it has been postulated that the presence of two NMR signals for glucose residues is due to a packing effect in the B-polymorph amylose crystal[17,42]. The complete attribution, realised by Rondeau-Mouro *et al.*, has been done on a highly crystalline material. In order to take this periodicity property into account, the determination of the theoretical NMR parameters was carried out under PBC using the GIPAW method.

As in our previous analysis on molecular systems, two types of conformation have been considered to model the two hydrogen bonds networks (HBN_1 and HBN_2) previously highlighted. For PBC calculations, geometry optimizations were performed considering the entire set of atoms. In this case, constrained geometry optimizations restrained to hydrogen atoms have not been considered because PBC induce crystal packing constraints. According to the 3D structure (Figure 5), two pseudo-axis of third (rotation- translation axis 3_1) and sixth (rotation-translation axis 6_1) order rotational symmetry determine the repartition of each helix within the crystal. One double helix has three close neighbors distributed according to the third order rotational axis. Thus, two populations of residues can be differentiated along amylose chains regarding their positions inside the crystal (Figure 5). One type of sugar is located at the interface between two amylose double helices (sugar in blue color in Figure 5 and noted $sugar_{interface}$) while the other corresponds to sugars that point toward the sixth order rotational axis (sugar in orange color in Figure 5 and noted $sugar_{solvent}$). These last sugars are in contact with structural water molecules that have been characterized in the solvent channel within the crystal structure[42]. It is know that the hydrogen bonding interaction of water molecules with hydroxyl groups attached to glucose moieties can have an impact on the values of ^{13}C chemical shifts[16,64]. However, these water molecules have not been taken into account in our calculations, considering the difficulty to

unambiguously place their hydrogen atoms. The principal dihedral angles for both structures and optimization strategies are presented in Table 3.

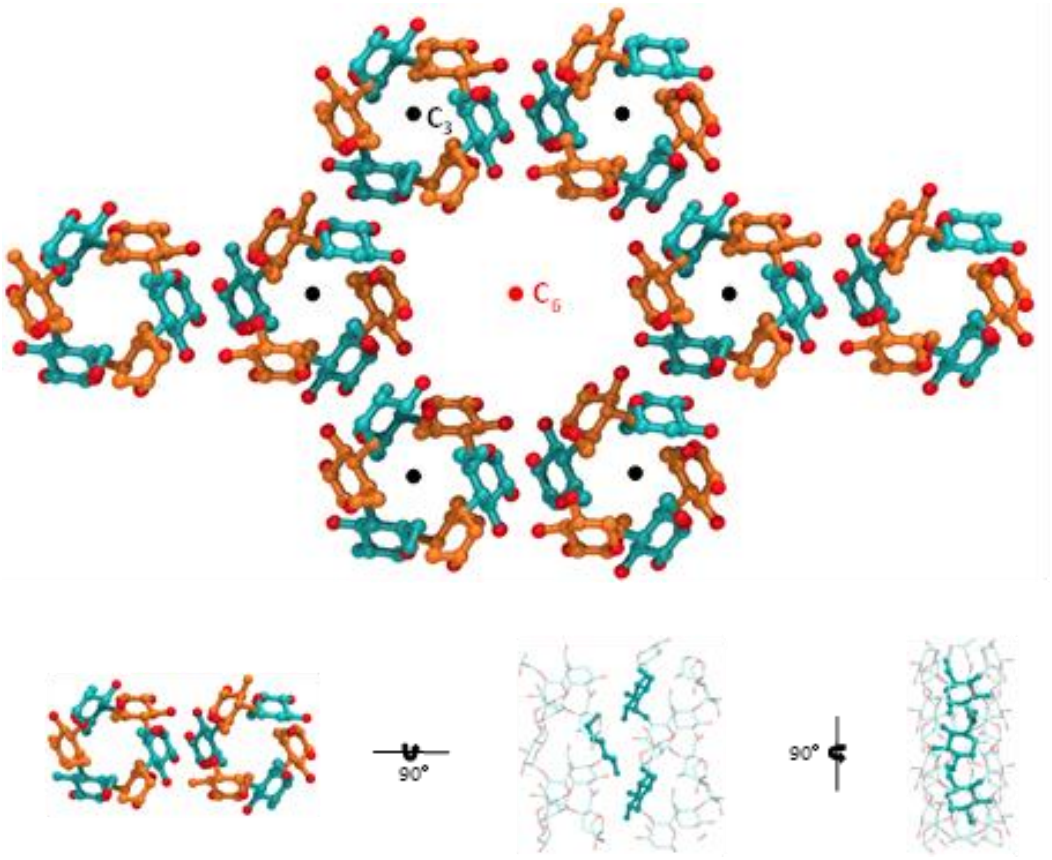

Figure 5. Up: Localisation of $sugar_{interface}$ (blue) and $sugar_{solvent}$ (orange) in the extended crystal mesh. In the crystal unit, C_3 is the rotation-translation axis 3_1 and the inertial axis of a double-helix, C_6 is the rotation-translation axis 6_1 and director axis of the crystal solvent channel.

	HBN_1	HBN_2	HNB_3	HNB_4
O_5-C_1-O_4'-C_4'	**81.7** 90.6	90.8 88.9	87.4 82.8	79.7 92.9
C_1-O_4'-C_4'-C_3'	97.8 94.5	96.4 98.0	92.8 97.4	95.7 96.6
C_4-C_5-C_6-O_6	51.4 67.9	54.9 60.5	57.3 62.2	59.2 61.1
C_1-C_2-O_2-H_{o2}	249.8 247.5	33.5 **120.1**	281.3 288.7	267.7 265.2
C_2-C_3-O_3-H_{o3}	192.1 177.5	294.9 308.1	313.6 300.6	**189.3** 292.8
C_5-C_6-O_6-H_{o6}	**17.4** 280.5	129.3 147.0	16.9 290.0	14.3 295.1

Table 3. Selected averaged dihedral angles (degrees) of the full optimisations, using PBC, resulting in the HBN_1, HBN_2, HBN_3 and HBN_4 structures (See text for details). O_5-C_1-O_4'-C_4' and C_1-O_4'-C_4'-C_3' are the φ and ψ angles, respectively. For each angle, the first value corresponds to the $sugar_{interface}$, the second to the $sugar_{solvent}$. In bold, dihedral angle values out of range of values defined by molecular approach.

As for the molecular approach, the nature of the hydrogen bond network has little influence on the values of the dihedral angles that defined the conformation around the C_5-C_6 bonds (mainly *gg* type). For the glycosidic angles φ and ψ, a similar conclusion is reached, even if a difference of 10° is observed for the φ angle of the residue at the interface when one goes from HBN_1 to HBN_2 (81.7° to 90.8°, respectively). When other structural parameters are considered, two sets of values are obtained for all dihedral angles reflecting this differentiation between residues. Moreover, if compared with the previous hydrogen bond networks (molecular approach-HBN_1,

characterised by C_1-C_2-O_2-H_{O2}, C_2-C_3-O_3-H_{O3}, C_5-C_6-O_6-H_{O6} ranging from 200° to 280°, 180° to 215° and 280° to 290°; molecular approach-HBN_2, characterised by C_1-C_2-O_2-H_{O2}, C_2-C_3-O_3-H_{O3}, C_5-C_6-O_6-H_{O6} ranging from 25° to 50°, 290° to 310° and 135° to 165°), while there are similarities for dihedral angles, the ones resulting from PBC calculations present differences (Figure 6 and Table 3) due to interactions between helices.

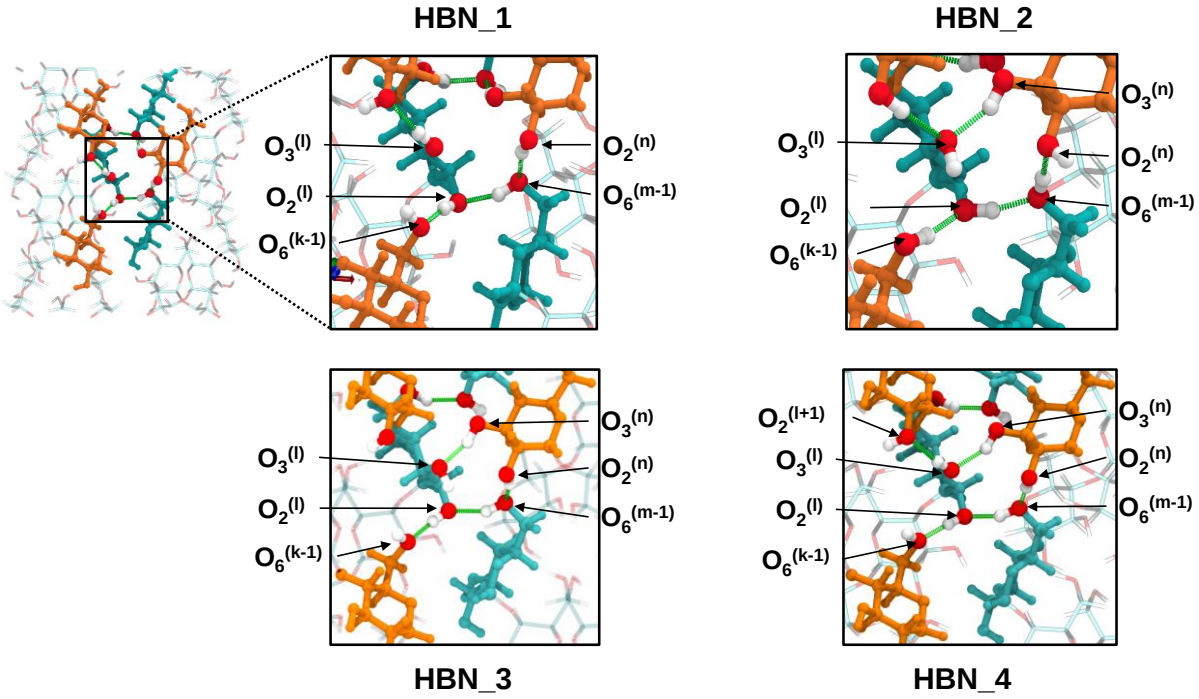

Figure 6. Details of HBN_1, HBN_2, HBN_3 and HBN_4 structures resulting from full geometry optimisations in periodic boundary conditions.

In the case of HBN_1, difference between the two types of sugar is observed for the dihedral angle around the C_6-O_6 bonds, while for HBN_2, this difference is observed for the conformation around the C_2-O_2 bond. In both cases, the difference in dihedral angle values is around 90 degrees. This can be related to the formation of slightly different hydrogen bond networks compare to molecular approach. The HBN_1 is now formed by hydrogen bonds between $H_{O2}^{(n)}$ and $O_6^{(m-1)}$,

$H_{O6}^{(m-1)}$ and $O_2^{(l)}$, $H_{O2}^{(l)}$ and $O_6^{(k-1)}$, with m and n referring to residues of different chains situated in the same double helix, k and l referring to residues of different chains situated in another double helix (Figure 6 HBN_1). The hydrogen bonds formed between $H_{O3}^{(n \text{ or } l)}$ and $O_2^{(n+1 \text{ or } l+1)}$ are conserved along the helix with no variation dependent on the position of the considered residue. The HBN_2 is formed by hydrogen bonds between $H_{O6}^{(k-1)}$ and $O_2^{(l)}$, $H_{O2}^{(l)}$ and $O_6^{(m-1)}$, $H_{O6}^{(m-1)}$ and $O_2^{(n)}$, $H_{O2}^{(l+1)}$ and $O_3^{(l)}$, $H_{O3}^{(n)}$ and $O_3^{(l)}$ (Figure 6 HBN_2). In the latter case, the O_3 of $sugars_{solvent}$ are only hydrogen bond donor (Figure 6 HBN_2, $O_3^{(n)}$) whereas O_3 of $sugars_{interface}$ are acceptors of two hydrogen bonds (Figure 6 HBN_1, $O_3^{(k)}$). Thus, HO_3 hydroxyl groups can be differentiated in the HBN_2 from $sugar_{interface}$ to $sugar_{solvent}$ using their intrinsic number of hydrogen bonds. This differentiation is not possible in the HBN_1 structure.

It has been demonstrated in monosaccharide systems that the number and nature of hydrogen bond formed on a C_i carbon have a direct impact on the calculated chemical shift of carbons C_{i+1} and C_{i-1}[15]. As a consequence, chemical shieldings have been calculated for the sugar carbon atoms in the crystal structures using PBC and compared to experiment. First, two populations of residues were differentiated in terms of chemical shielding (Figure S2) for both HBN_1 and HBN_2 geometrically optimized structures. One is associated to sugars located at the interface between double-helices ($sugar_{interface}$) while the other corresponds to the other family of sugar facing the solvent channel ($sugar_{solvent}$). This observation seems to confirm the experimental hypothesis about the differentiation of two sugars due to crystal packing. The next question is whether these two sets of ^{13}C chemical shieldings ($sugar_{interface}$ and $sugar_{solvent}$) calculated for the HBN structures can be directly associated to the two sets of experimental data (Sugar 1 and Sugar 2). Using the 4 possible combinations ([$sugar_{interface}$, $sugar_{solvent}$] vs [sugar 1, sugar 2] for the geometrical structures HBN_1 and 2, see Table S9), it was not possible to find a global correlation (i.e., using

simultaneously the 12 experimental carbon chemical shifts) between the theoretical and experimental data. The best correlations are displayed in Table 4 and Figure 7 (R^2 =0.985-986; RMSD=1.4 ppm). On the basis of the structures HBN_1 and HBN_2 that we have defined, it is not then possible to associate directly the structural position of sugar (facing a double helix or solvent) with one type of sugar identified experimentally. However, if we consider the relative errors associated with the twelve carbon chemical shifts (Figure 7), we observe that the $sugar_{interface}$ with HBN_1 hydrogen bonds (Figure 7a Sugar 1, blue bars) presents lower absolute values (< 1.5 ppm) than when they are involved with HBN_2 hydrogen bonds (Figure 7a Sugar 2, red bars, <3.2 ppm). On the contrary, $sugar_{solvent}$ presents smaller absolute relative error values in the HBN_2 structure (Figure 7a Sugar 1, red bars) than in HBN_1 structure (Figure 7a Sugar 2, blue bars) with maximum at 1.9 ppm compared to 3.6 ppm, respectively. These results suggest that one homogeneous hydrogen bond orientation replicated along the entire amylose chains does not form a viable model for the calculation of NMR parameters of such complexes. Because fast exchange between the two hydrogen bond networks can be present, dynamical effects must be somehow taken into account. In order to statically model the latter, the averaging of chemical shifts has been considered. Mean values have been calculated for each carbon by averaging chemical shifts of HBN_1 and HBN_2. Comparison with experimental data shows that the new sets of 12 chemical shifts (average_1 and average_2 in Table 4) substantially improved our theoretical results with excellent correlation coefficient (R^2=0.994) and RMSD (< 1 ppm). In addition, the errors are more evenly distributed over all carbons with values below 2 ppm (Figure 7b). However, the discrimination between $sugar_{interface}$ and $sugar_{solvent}$ remains impossible (see for example all C_1 values for average_1 and 2 in Table 4). This average of HBN_1 and HBN_2 can be considered as

a static model of a synchronous dynamic of both hydrogen bond networks, i.e., the whole hydrogen bond network moves from HBN_1 to HBN_2.

		Exp.[17]	HBN_1		HBN_2		average 1		average 2		HBN_3		HBN_4	
Sugar 1	**C1**	**99.3**	99.2	$Sugar_{interface}$	100.0	$Sugar_{solvent}$	99.5	$Sugar_{interface}$	99.5	$Sugar_{solvent}$	99.7	$Sugar_{interface}$	99.2	$Sugar_{solvent}$
	C2	**71.3**	70.9		71.2		71.2		73.2		72.2		74.0	
	C3	**75.1**	75.7		74.4		73.5		75.1		73.8		74.9	
	C4	**72.6**	73.9		74.5		74.1		73.4		71.6		72.3	
	C5	**69.8**	70.0		70.5		71.1		70.6		70.6		69.1	
	C6	**61.3**	59.8		61.0		60.7		60.5		61.9		61.4	
Sugar 2	**C1**	**100.2**	98.5	$Sugar_{solvent}$	99.4	$Sugar_{interface}$	99.5	$Sugar_{solvent}$	99.5	$Sugar_{interface}$	100.1	$Sugar_{solvent}$	100.1	$Sugar_{interface}$
	C2	**72.1**	75.3		71.5		73.2		71.2		73.9		70.2	
	C3	**75.1**	75.8		71.5		75.1		73.5		75.0		74.1	
	C4	**74.3**	72.4		74.3		73.4		74.1		73.4		74.3	
	C5	**70.2**	70.8		72.4		70.6		71.1		69.0		71.6	
	C6	**61.3**	60.3		61.9		60.5		60.7		61.5		61.4	
R^2			**0.986**		**0.985**		**0.994**		**0.994**		**0.994**		**0.991**	
RMSD			**1.4**		**1.4**		**0.9**		**0.9**		**0.9**		**1.1**	

Table 4. Best calculated chemical shifts (ppm) for HBN_1, HBN_2 HBN_3 and HBN_4 theoretical structures after correction with experimental data using the coefficients of the linear interpolation (experiment vs theory, see methods). Chemical shifts (average_1 and 2) obtained after averaging of $sugar_{interface}$ or $sugar_{solvent}$ chemical shieldings of HBN_1 and HBN_2 optimized structures and correction with experimental data using the coefficients of the linear interpolation are also calculated. R^2 and RMSD (in ppm) are given in order to indicate an estimation of errors.

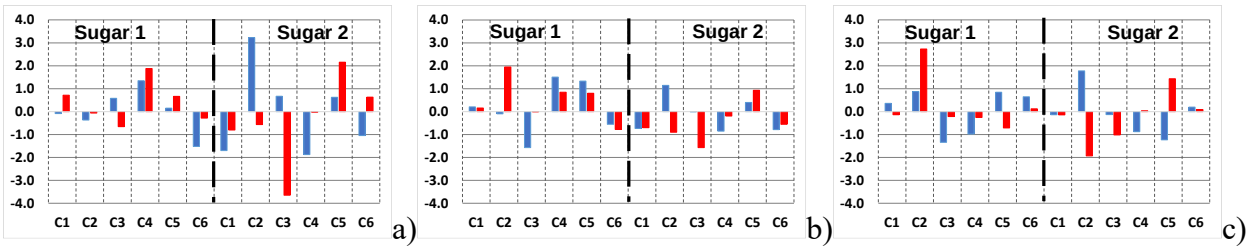

Figure 7. Relative errors (ppm) resulting from the best theory/experiment correlations for (a) HBN_1 (Blue) and HBN_2 (Red), (b) for average_1 (Blue) and average_2 (Red) and (c) HBN_3 (Blue) and HBN_4 (Red).

An asynchronous dynamic can be envisaged for which only the hydrogen bond network of one type of sugar is modified (either $sugar_{interface}$ or $sugar_{solvent}$). To confirm this hypothesis, we constructed two other hydrogen bond networks: The first, noted HBN_3, presents HBNs for the $sugar_{interface}$ and $sugar_{solvent}$ close to HBN_2 and HBN_1, respectively. The second, noted HBN_4 on the contrary, presents HBNs for the $sugar_{interface}$ and $sugar_{solvent}$ close to HBN_1 and HBN_2, respectively. The two resulting structures were subjected to geometry optimization and chemical shieldings were calculated and compared to experiment (see Table 4). The carbon skeletons do not show specific alteration for the two new considered structures if φ, ψ and dihedral angles around C_5-C_6 are considered (Table 3). Concerning the hydrogen bond networks, only the dihedral angles around C_6-O_6 can discriminate the two sugars (interfacial and facing to solvent) for HNB_3 while for HNB_4, dihedral angles around C_6-O_6 and C_3-O_3 allow to differentiate the two positions. As already described in the previous paragraphs, these reflect difference of hydrogen bonding between helices both in intra and inter double-helix, within the crystal lattice and can be at the origin of different chemical shifts repartition calculated for these structures.

For HBN_3 and HBN_4 structures, global correlation of NMR chemical shielding has been envisaged by correlating at the same time $sugar_{interface}$ with sugar 1 and $sugar_{solvent}$ with sugar 2 or

the opposite (Table S10). The best correlations are displayed in Table 4. For HBN_3, the best results are obtained by assigning chemical shifts of $sugar_{interface}$ and $sugar_{solvent}$ to Sugar 1 and 2 respectively, while for HBN_4 the opposite has been found, $sugar_{interface}$ and $sugar_{solvent}$ being correlated to Sugar 2 and 1, respectively. Even though several little errors remain (Figure 7c error < 1.8 and 2.7 ppm for HBN_3 and 4 structures, respectively), these values yield also a very good agreement compared to experiment. The corresponding correlation coefficients (0.994 and 0.991) together with RMSD around 1 ppm calculated using the whole set of chemical shifts are a proof of this correctness. However, for one of these structures, Sugar 1 is attributed to sugars at the interface between double-helices while for the other, the same experimental sugar is attributed to sugars facing the solvent channel.

Conclusions.

In conclusion, we demonstrate that it is possible to achieve qualitative good agreement between experiment and theoretical ^{13}C NMR chemical shifts in the case of a highly crystalline sample of the Amylose B-polymorph. To do so, it is necessary to correctly model the chemical environment using calculations at the DFT level within periodic boundary conditions. This was necessary to confirm, for the first time, the experimental hypothesis that the presence of two types of sugar in the NMR spectrum is a consequence of crystal packing.

However, neither of the theoretical structures allow us to discriminate the assignment of NMR spectra with respect to the position of the sugars. It is necessary to remember that no water molecules are included in our calculations, especially those that have been characterised in a specific channel created by the six double-helices distributed around the C_6 pseudo axis. These water molecules are crucial for the crystal structure of the B-polymorph of amylose[42] and

obviously may play an important role in the evaluation of ^{13}C NMR chemical shifts. They may create new dynamic hydrogen bonds with the hydroxyl groups of the residues located in this channel and thus influence the value of chemical shielding of carbons C_2, C_3 and C_5. Because the position of the hydrogen atoms of water is not characterised by X-ray scattering, it is impossible to correctly model these molecules in our computational strategy without resorting to *ab initio* molecular dynamics, which is outside the scope of this study.

Supporting Information.

The supporting information is available free of charge. Table S1: φ and ψ angles after geometry optimizations and for the crystal structure; Table S2: Selected dihedral angles for full (all atoms) geometry optimizations; Table S3: Selected dihedral angles for constrained (Hydrogen atoms only) geometry optimizations; Table S4: φ and ψ angles averages extracted from MD simulation; Table S5: Selected dihedral angles averages extracted from MD simulation; Table S6: Chemical shielding obtained for full (all atoms) geometry optimizations methods; Table S7: Chemical shielding obtained for constrained (hydrogen atoms only) geometry optimizations method; Table S8: Molecular approach. Experimental chemical shift and average theoretical chemical shielding used for theory vs experience comparison and parameters of the linear fit; Table S9: Periodic Boundary conditions approach. Experimental chemical shift and theoretical chemical shielding used for theory vs experience comparison; Table S10: Periodic Boundary conditions approach. Experimental chemical shift and theoretical chemical shielding used for theory vs experience comparison; Figure S1: Energy difference as a function of k-points grid sampling. Figure S2: Carbon chemical Shielding obtained after GIPAW calculations on HBN_1 and HBN_2 optimized structures;

Corresponding Author

*Franck Jolibois. E-Mail: franck.jolibois@univ-tlse3.fr

Author Contributions

The manuscript was written through contributions of all authors. All authors have given approval to the final version of the manuscript.

ACKNOWLEDGMENT

A.S. was a recipient of a PhD scholarship from University of Toulouse and the "Région Occitanie". This work was supported by the CNRS-MITI grant "Modélisation du vivant" 2019. This work was granted access to the HPC resources of CALMIP supercomputing centre under the allocation 2018-p0758 and of CINES and IDRIS supercomputing centre under the allocation 2019-A0060810816 made by GENCI.

REFERENCES

(1) Rappenecker, G.; Zugenmaier, P. Detailed Refinement of the Crystal Structure of Vh-Amylose. *Carbohydr. Polym.* **1981**, *89*, 11–19.

(2) Winter, W. T.; Sarko, A. Crystal and Molecular Structure of the Amylose-DMSO Complex. *Biopolymers* **1974**, *13*, 1461–1482.

(3) Takahashi, Y.; Kumano, T.; Nishikawa, S. Crystal Structure of B-Amylose. *Macromolecules* **2004**, *37*, 6827–6832.

(4) Murphy, V. G.; Zaslow, B.; French, A. D. The Structure of V Amylose Dehydrate : A Combined X-Ray and Stereochemical Approach. *Biopolymers* **1975**, *14*, 1487–1501.

(5) Immel, S.; Lichtenthaler, F. W. The Hydrophobic Topographies of Amylose and Its Blue Iodine Complex. *Starch - Stärke* **2002**, *52*, 1–8.

(6) Nuessli, J.; Putaux, J. L.; Le Bail, P.; Buléon, A. Crystal Structure of Amylose Complexes with Small Ligands. *Int. J. Biol. Macromol.* **2003**, *33*, 227–234.

(7) Tapanapunnitikul, O.; Chaiseri, S.; Peterson, D. G.; Thompson, D. B. Water Solubility of Flavor Compounds Influences Formation of Flavor Inclusion Complexes from Dispersed High-Amylose Maize Starch. *J. Agric. Food Chem.* **2008**, *56*, 220–226.

(8) Eliasson, A. C.; Krog, N. Physical Properties of Amylose-Monoglyceride Complexes. *J. Cereal Sci.* **1985**, *3*, 239–248.

(9) F. Horii, H. Yamamoto, A. Hirai, R. K. Structural Study of Amylose Polymorphs by Cross-Polarization-Magic-Angle Spinning, 13C-N.M.R. Spectroscopy. *Carbohydr. Res.* **1987**, *160*, 29–40.

(10) Lebail, P.; Buleon, A.; Shiftan, D.; Marchessault, R. H. Mobility of Lipid in Complexes of Amylose-Fatty Acids by Deuterium and 13C Solid State NMR. *Carbohydr. Polym.* **2000**, *43*, 317–326.

(11) Gelders, G. G.; Vanderstukken, T. C.; Goesaert, H.; Delcour, J. A. Amylose-Lipid Complexation: A New Fractionation Method. *Carbohydr. Polym.* **2004**, *56*, 447–458.

(12) Gidley, M. J. Quantification of the Structural Features of Starch Polysaccharides by NMR Spectroscopy. *Carbohydr. Res.* **1985**, *139*, 85–93.

(13) Snape, C. E.; Morrison, W. R.; Maroto-Valer, M. M.; Karkalas, J.; Pethrick, R. A. Solid

State 13C NMR Investigation of Lipid Ligands in V-Amylose Inclusion Complexes. *Carbohydr. Polym.* **1998**, *36*, 225–237.

(14) Duus, J.; Gotfredsen, C. H.; Bock, K. Carbohydrate Structural Determination by NMR Spectroscopy: Modern Methods and Limitations. *Chem. Rev.* **2000**, *100*, 4589–4614.

(15) Suzuki, S.; Horii, F.; Kurosu, H. Theoretical Investigations of 13C Chemical Shifts in Glucose, Cellobiose, and Native Cellulose by Quantum Chemistry Calculations. *J. Mol. Struct.* **2009**, *921*, 219–226.

(16) Jolibois, F.; Soubias, O.; Réat, V.; Milon, A. Understanding Sterol-Membrane Interactions Part I: Hartree-Fock versus DFT Calculations of 13C and 1H NMR Isotropic Chemical Shifts of Sterols in Solution and Analysis of Hydrogen-Bonding Effects. *Chem. - A Eur. J.* **2004**, *10*, 5996–6004.

(17) Rondeau-Mouro, C.; Veronese, G.; Buléon, A. High-Resolution Solid-State NMR of B-Type Amylose. *Biomacromolecules* **2006**, *7*, 2455–2460.

(18) Kirschner, K. N.; Yongye, A. B.; Tschampel, S. M.; González-Outeiriño, J.; Daniels, C. R.; Foley, B. L.; Woods, R. J. GLYCAM06: A Generalizable Biomolecular Force Field. Carbohydrates. *J. Comput. Chem.* **2008**, *29*, 622–655.

(19) Guvench, O.; Mallajosyula, S. S.; Raman, E. P.; Hatcher, E.; Vanommeslaeghe, K.; Foster, T. J.; Jamison, F. W.; MacKerell, A. D. CHARMM Additive All-Atom Force Field for Carbohydrate Derivatives and Its Utility in Polysaccharide and Carbohydrate-Protein Modeling. *J. Chem. Theory Comput.* **2011**, *7*, 3162–3180.

(20) Plazinski, W.; Lonardi, A.; Hünenberger, P. H. Revision of the GROMOS 56A6 CARBO Force Field: Improving the Description of Ring-Conformational Equilibria in Hexopyranose-Based Carbohydrates Chains. *J. Comput. Chem.* **2016**, *37*, 354–365.

(21) Tusch, M.; Krüger, J.; Fels, G. Structural Stability of V-Amylose Helices in Water-DMSO Mixtures Analyzed by Molecular Dynamics. *J. Chem. Theory Comput.* **2011**, *7*, 2919–2928.

(22) Koneru, J. K.; Zhu, X.; Mondal, J. Quantitative Assessment of the Conformational Heterogeneity in Amylose across Force Fields. *J. Chem. Theory Comput.* **2019**, *15*, 6203–6212.

(23) López, C. A.; De Vries, A. H.; Marrink, S. J. Amylose Folding under the Influence of Lipids. *Carbohydr. Res.* **2012**, *364*, 1–7.

(24) Feng, T.; Li, M.; Zhou, J.; Zhuang, H.; Chen, F.; Ye, R.; Campanella, O.; Fang, Z. Application of Molecular Dynamics Simulation in Food Carbohydrate Research - A Review. *Innov. Food Sci. Emerg. Technol.* **2015**, *31*, 1–13.

(25) Cheng, L.; Feng, T.; Zhang, B.; Zhu, X.; Hamaker, B.; Zhang, H.; Campanella, O. A Molecular Dynamics Simulation Study on the Conformational Stability of Amylose-Linoleic Acid Complex in Water. *Carbohydr. Polym.* **2018**, *196*, 56–65.

(26) Cheng, L.; Zhu, X.; Hamaker, B. R.; Zhang, H.; Campanella, O. H. Complexation Process of Amylose under Different Concentrations of Linoleic Acid Using Molecular Dynamics Simulation. *Carbohydr. Polym.* **2019**, *216*, 157–166.

(27) Toukach, F. V.; Ananikov, V. P. Recent Advances in Computational Predictions of NMR

Parameters for the Structure Elucidation of Carbohydrates: Methods and Limitations. *Chem. Soc. Rev.* **2013**, *42*, 8376–8415.

(28) Kubicki, J. D.; Mohamed, M. N.-A.; Watts, H. D. Quantum Mechanical Modeling of the Structures, Energetics and Spectral Properties of Iα and Iβ Cellulose. *Cellulose* **2013**, *20*, 9–23.

(29) Yang, H.; Wang, T.; Oehme, D.; Petridis, L.; Hong, M.; Kubicki, J. D. Structural Factors Affecting 13C NMR Chemical Shifts of Cellulose: A Computational Study. *Cellulose* **2018**, *25*, 23–36.

(30) Esrafili, M. D.; Ahmadin, H. DFT Study of 17O, 1H and 13C NMR Chemical Shifts in Two Forms of Native Cellulose, Iα and Iβ. *Carbohydr. Res.* **2012**, *347*, 99–106.

(31) Schahl, A.; Réat, V.; Jolibois, F. Structures and NMR Spectra of Short Amylose-Lipid Complexes. Insight Using Molecular Dynamics and DFT Quantum Chemical Calculations. *Carbohydr. Polym.* **2020**, *235*, 115846.

(32) Wolinski, K.; Hinton, J. F.; Pulay, P. Efficient Implementation of the Gauge-Independent Atomic Orbital Method for NMR Chemical Shift Calculations. *J. Am. Chem. Soc.* **1990**, *112*, 8251–8260.

(33) Pickard, C. J.; Mauri, F. All-Electron Magnetic Response with Pseudopotentials: NMR Chemical Shifts. *Phys. Rev. B* **2001**, *63*, 245101–245113.

(34) Yates, J. R.; Pickard, C. J.; Mauri, F. Calculation of NMR Chemical Shifts for Extended Systems Using Ultrasoft Pseudopotentials. *Phys. Rev. B* **2007**, *76*, 024401–024411.

(35) Marín-Luna, M.; Alkorta, I.; Elguero, J. A Theoretical NMR Study of Selected Benzazoles: Comparison of GIPAW and GIAO-PCM (DMSO) Calculations. *Magn. Reson. Chem.* **2018**, *56*, 164–171.

(36) Gerber, I. C.; Jolibois, F. Theoretical Gas to Liquid Shift of 15N Isotropic Nuclear Magnetic Shielding in Nitromethane Using Ab Initio Molecular Dynamics and GIAO/GIPAW Calculations. *Phys. Chem. Chem. Phys.* **2015**, *17*, 12222–12227.

(37) De Souza, F. A. L.; Ambrozio, A. R.; Souza, E. S.; Cipriano, D. F.; Scopel, W. L.; Freitas, J. C. C. NMR Spectral Parameters in Graphene, Graphite, and Related Materials: Ab Initio Calculations and Experimental Results. *J. Phys. Chem. C* **2016**, *120*, 27707–27716.

(38) Zurek, E.; Pickard, C. J.; Autschbach, J. A Density Functional Study of the 13C NMR Chemical Shifts in Functionalized Single-Walled Carbon Nanotubes. *J. Am. Chem. Soc.* **2007**, *129*, 4430–4439.

(39) Zurek, E.; Pickard, C. J.; Walczak, B.; Autschbach, J. Density Functional Study of the 13C NMR Chemical Shifts in Small-to-Medium-Diameter Infinite Single-Walled Carbon Nanotubes. *J. Phys. Chem. A* **2006**, *110*, 11995–12004.

(40) Phillips, J. C.; Braun, R.; Wang, W.; Gumbart, J.; Tajkhorshid, E.; Villa, E.; Chipot, C.; Skeel, R. D.; Kalé, L.; Schulten, K. Scalable Molecular Dynamics with NAMD. *J. Comput. Chem.* **2005**, *26*, 1781–1802.

(41) Case, D. A.; Cheatham, T. E.; Darden, T.; Gohlke, H.; Luo, R.; Merz, K. M.; Onufriev, A.; Simmerling, C.; Wang, B.; Woods, R. J. The Amber Biomolecular Simulation Programs. *J. Comput. Chem.* **2005**, *26*, 1668–1688.

(42) Imberty, A.; Pérez, S. A Revisit to Three-Dimensional Structure of B-Type Starch. *Biopolymers* **1988**, *27*, 1205–1221.

(43) Hanwell, M. D.; Curtis, D. E.; Lonie, D. C.; Vandermeerschd, T.; Zurek, E.; Hutchison, G. R. Avogadro: An Advanced Semantic Chemical Editor, Visualization, and Analysis Platform. *J. Cheminform.* **2012**, *4*, 1–17.

(44) Virtanen, P.; Gommers, R.; Oliphant, T. E.; Haberland, M.; Reddy, T.; Cournapeau, D.; Burovski, E.; Peterson, P.; Weckesser, W.; Bright, J.; van der Walt, S. J.; Vázquez-Baeza, Y.; et al. SciPy 1.0: Fundamental Algorithms for Scientific Computing in Python. *Nat. Methods* **2020**, *17*, 261–272.

(45) Frisch, M. J.; Trucks, G. W.; Schlegel, H. B.; Scuseria, G. E.; Robb, M. A.; Cheeseman, J. R.; Scalmani, G.; Barone, V.; Petersson, G. A.; Nakatsuji, H.; et al. Gaussian 09, Revision A.02. *Gaussian, Inc., Wallingford CT* **2016**, 2016.

(46) Becke, A. D. Density-Functional Thermochemistry. III. The Role of Exact Exchange. *J. Chem. Phys.* **1993**, *98*, 5648–5652.

(47) Lee, C.; Yang, W.; Parr, R. G. Development of the Colle-Salvetti Correlation-Energy Formula into a Functional of the Electron Density. *Phys. Rev. B* **1988**, *37*, 785–789.

(48) Krishnan, R.; Binkley, J. S.; Seeger, R.; Pople, J. A. Self-Consistent Molecular Orbital Methods. XX. A Basis Set for Correlated Wave Functions. *J. Chem. Phys.* **1980**, *72*, 650–654.

(49) McLean, A. D.; Chandler, G. S. Contracted Gaussian Basis Sets for Molecular Calculations.

I. Second Row Atoms, Z=11-18. *J. Chem. Phys.* **1980**, *72*, 5639–5648.

(50) Ditchfield, R. Molecular Orbital Theory of Magnetic Shielding and Magnetic Susceptibility. *J. Chem. Phys.* **1972**, *56*, 5688–5691.

(51) Miertuš, S.; Scrocco, E.; Tomasi, J. Electrostatic Interaction of a Solute with a Continuum. A Direct Utilizaion of AB Initio Molecular Potentials for the Prevision of Solvent Effects. *Chem. Phys.* **1981**, *55*, 117–129.

(52) Sarkar, A.; Pérez, S. PolySac3DB: An Annotated Data Base of 3 Dimensional Structures of Polysaccharides. *BMC Bioinformatics* **2012**, *13*, 302.

(53) Kresse, G.; Furthmüller, J. Efficiency of Ab-Initio Total Energy Calculations for Metals and Semiconductors Using a Plane-Wave Basis Set. *Comput. Mater. Sci.* **1996**, *6*, 15–50.

(54) Kresse, G.; Hafner, J. Ab Initio Molecular Dynamics for Liquid Metals. *Phys. Rev. B* **1993**, *47*, 558–561.

(55) Kresse, G.; Furthmüller, J. Efficient Iterative Schemes for Ab Initio Total-Energy Calculations Using a Plane-Wave Basis Set. *Phys. Rev. B* **1996**, *54*, 11169–11186.

(56) Kresse, G.; Hafner, J. Ab Initio Molecular-Dynamics Simulation of the Liquid-Metalamorphous- Semiconductor Transition in Germanium. *Phys. Rev. B* **1994**, *49*, 14251–14269.

(57) Blöchl, P. E. Projector Augmented-Wave Method. *Phys. Rev. B* **1994**, *50*, 17953–17979.

(58) Kresse, G.; Joubert, D. From Ultrasoft Pseudopotentials to the Projector Augmented-Wave Method. *Phys. Rev. B* **1999**, *59*, 1758–1775.

(59) Perdew, J. P.; Burke, K.; Ernzerhof, M. Generalized Gradient Approximation Made Simple. *Phys. Rev. Lett.* **1996**, *77*, 3865–3868.

(60) Grimme, S.; Antony, J.; Ehrlich, S.; Krieg, H. A Consistent and Accurate Ab Initio Parametrization of Density Functional Dispersion Correction (DFT-D) for the 94 Elements H-Pu. *J. Chem. Phys.* **2010**, *132*, 154104–154119.

(61) Vasconcelos, F.; De Wijs, G. A.; Havenith, R. W. A.; Marsman, M.; Kresse, G. Finite-Field Implementation of NMR Chemical Shieldings for Molecules: Direct and Converse Gauge-Including Projector-Augmented-Wave Methods. *J. Chem. Phys.* **2013**, *139*, 014109–014116.

(62) Marchessault, R. H.; Perez, S. Conformations of the Hydroxymethyl Group in Crystalline Aldohexopyranoses. *Biopolymers* **1979**, *18*, 2369–2374.

(63) Nishida, Y.; Ohrui, H.; Meguro, H. 1H-NMR Studies of (6R)- and (6S)-Deuterated D-Hexoses: Assignment of the Preferred Rotamers About C5-C6 Bond of D-Glucose AND D-Galactose Derivatives in Solutions. *Tetrahedron Lett.* **1984**, *25*, 1575–1578.

(64) Bagno, A.; Rastrelli, F.; Saielli, G. Prediction of the 1H and 13C NMR Spectra of α-D-Glucose in Water by DFT Methods and MD Simulations. *J. Org. Chem.* **2007**, *72*, 7373–7381.

TOC Graphic

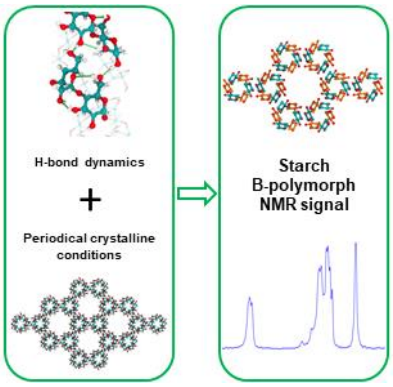
H-bond dynamics
+
Periodical crystalline conditions
Starch
B-polymorph
NMR signal